Transdisciplinary Engineering Methods for Social Innovation of Industry 4.0
M. Peruzzini et al. (Eds.)

doi:10.3233/978-1-61499-898-3-693

Geometrical Optimization of Axially Loaded Tubular Adhesive Joints by Finite Elements

L.R.F. FERREIRA[a], R.D.S.G. CAMPILHO[a,b, 1] and D.R. BARBOSA[a]
[a] *Departamento de Engenharia Mecânica, Instituto Superior de Engenharia do Porto, Instituto Politécnico do Porto, Rua Dr. António Bernardino de Almeida, 431, 4200-072 Porto, Portugal*
[b] *INEGI – Pólo FEUP, Rua Dr. Roberto Frias, s/n, 4200-465 Porto, Portugal*

Abstract. Bonding with adhesives is increasingly being used in the design of mechanical structures. Tubular joints find applications in the piping industry, vehicle frames or thin-walled tubes, for instance, but they are seldom studied in the literature. This work numerically addressed the tensile strength of aluminum tubular joints, after validation of the numerical tool with experiments. The numerical analysis consisted of using the Finite Element (FE) method and cohesive zone models (CZM) to predict the joint strength. Numerically, the effect of the overlap length (L_O) and the thickness of the inner and outer tubes (t_{SI} and t_{SE}, respectively) is addressed. The CZM technique was positively validated for the strength analysis of tubular joints. It was also shown that the joints' geometry and type of adhesive highly influence the joints' behaviour.

Keywords. Finite Elements; Cohesive Zone Models; Structural Adhesive; Tubular Joints; Geometric parameters.

Introduction

Adhesive bonding is one of the most used joining methods nowadays and is widely studied due to its potential. As a result of improvements in the characteristics of adhesives, adhesive bonding has progressively replaced traditional joining methods such as bolting or riveting [1]. The aeronautical industry was the pioneer of this technology. The automotive and rail industries have also resorted to adhesives in order to obtain lighter structures. Other examples include construction, shoe making and electronics [2].

The strength prediction of bonded joints historically began with analytical stress analyses and then evolved to numerical methods. The finite element method has been used since the 70's and eventually turned out to be the most used technique for the adhesive joints analysis. In the review of He [3], FE methods applied to bonded joints are extensively discussed. More traditionally, FE-based strength prediction can rely on continuum or fracture mechanics approaches. Currently, the most widespread technique is CZM, which includes both stress and toughness properties to characterize the progressive failure process of bonded joints [4, 5]. CZM modeling depends on accurate

[1] Corresponding author, Mail: raulcampilho@gmail.com.

values of cohesive strengths in tension and shear (t_n^0 and t_s^0, respectively), and tensile (G_{IC}) and shear toughness (G_{IIC}) [6].

In the industry, several adhesive joint configurations can be used. The most commonly used are single-lap joints, as they are the easiest to conceive and load the adhesive mainly in shear. However, since the adherends are not collinear, a bending moment appears that creates peel efforts. To overcome this problem, joggle-lap, stepped-lap or double-lap joints can be used instead, since these allow a more uniform distribution of stresses, reducing the peeling efforts [1]. In addition, butt joints, T-joints, corner joints and tubular adhesive joints can be used in more specific applications. Tubular joints in particular have a large bonded area and a higher flexural strength due to their overall stiffness [1]. The use of adhesives for tube joining is one of the most recurrent methods today, and this technique presents an extensive application in the piping industry. A few studies are available that deal with the analysis of tubular joints. Dragoni and Goglio [7] studied the accuracy of five theoretical models for the prediction of adhesive layer stresses produced by axial loads in tubular adhesive joints, and compared the results with the FEM. It was concluded that, within all models considered, only that of Lubkin and Reissner [8] gives a truthful distribution of the peel stress in the overlap.

This work numerically addressed the tensile strength of aluminum tubular joints, after validation of the numerical tool with experiments. The numerical analysis consisted of using the FE method and CZM to predict the joint strength. Numerically, the geometrical optimization addresses the effect of L_O and the thickness of the inner and outer tubes (t_{SI} and t_{SE}, respectively).

1. Experimental work

1.1. Materials

Tubular joints between AW6082 T651 aluminium alloy adherends were considered. The characterization of this alloy in bulk tension, following the standard ASTM-E8M-04, is detailed in [9]. The following mechanical properties were attained: Young's modulus (E) of 70.07±0.83 GPa, tensile yield stress (σ_y) of 261.67±7.65 MPa, tensile failure strength (σ_f) of 324±0.16 MPa and tensile failure strain (ε_f) of 21.70±4.24%.

Table 1. Mechanical and fracture properties of the adhesive Araldite® 2015 [10, 11].

Property	
Young's modulus, E [GPa]	1.85±0.21
Poisson's ratio, ν	0.33 [a]
Tensile yield stress, σ_y [MPa]	12.63±0.61
Tensile strength, σ_f [MPa]	21.63±1.61
Tensile failure strain, ε_f [%]	4.77±0.15
Shear modulus, G [GPa]	0.56±0.21
Shear yield stress, τ_y [MPa]	14.6±1.3
Shear strength, τ_f [MPa]	17.9±1.8
Shear failure strain, γ_f [%]	43.9±3.4
Toughness in tension, G_{IC} [N/mm]	0.43±0.02
Toughness in shear, G_{IIC} [N/mm]	4.70±0.34

[a] manufacturer's data

The ductile epoxy adhesive Araldite® 2015 was considered to fabricate the tubular joints. Mechanical and fracture characterization of this adhesive was properly undertaken in a previous works [10, 11]. The tensile mechanical properties were defined by tensile tests to bulk specimens, which enabled the estimation of E, σ_y, σ_f and ε_f. On the other hand, the Thick Adherend Shear Tests (TAST) was used for estimation of the shear mechanical properties, with C45E steel adherends. The relevant fracture properties of the adhesives (G_{IC} and G_{IIC}) were obtained from Double-Cantilever Beam (DCB) and End-Notched Flexure (ENF) tests, respectively [11, 12]. The adhesive's properties used in the simulations are described in Table 1.

1.2. Experimental details

Figure 1 represents the geometry of the tubular joints and the associated geometric parameters (dimensions in mm): L_O=20 and 40, adherends' free length L_S=50 for L_O=20 and 60 for L_O=40, joint free length L_T=80, outer diameter if the inner tube d_{SI}=20, outer diameter of the outer tube d_{SE}=22.4, t_{SI}=2, t_{SE}=2 and adhesive thickness t_A=0.2.

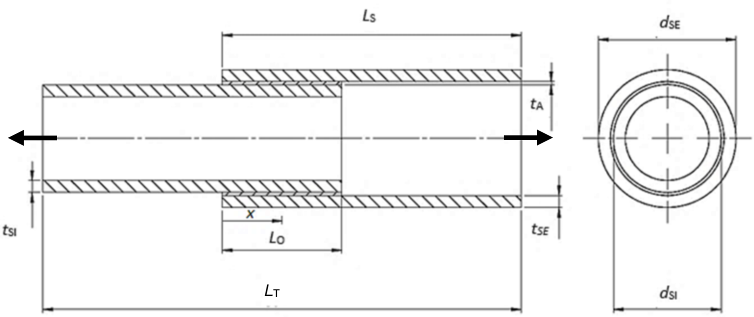

Figure 1. Geometry and characteristic dimensions of the tubular joints.

Testing of the specimens was carried out in a Shimadzu-Autograph AG-X tester, equipped with a 100 kN load cell, at room temperature and with a velocity of 1 mm/min. The tests resulted in individualized load-displacement (P-δ) curves that will enable comparison with the numerical results.

2. Numerical work

2.1. Simulation settings

The Abaqus® software was chosen to perform the CZM analysis of the tubular joints. The aluminium tubes were modelled using solid elasto-plastic elements, as per the σ-ε curves of reference [13]. CZM elements with a triangular mixed-mode law (further defined in this work) were used for the adhesive. Due to the particular characteristics of the tubular joints' geometry, i.e., with axisymmetric geometry, loads and boundary conditions, a two-dimensional (2D) axisymmetric FE study was considered. Figure 2 shows the mesh refinement for the tubular joint model with L_O=20 mm. In which concerns the applied boundary conditions, the tubes were clamped at one of the edges and pulled longitudinally while transversely restrained at the opposite edge.

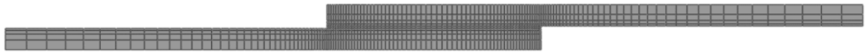

Figure 2. FE mesh detail of the axisymmetric model for a tubular with L_O=20 mm.

2.2. Traingular CZM model

CZM laws simulate the elastic behaviour up to a peak load and subsequent softening, to model the gradual degradation of material properties up to complete failure. The areas under the traction-separation laws in tension or shear are equalled to G_{IC} or G_{IIC}, respectively. Under pure mode, damage propagation occurs at a specific integration point when the stresses are released in the respective traction-separation law. Under mixed mode, energetic criteria are often used to combine tension and shear [14]. In this work, triangular pure and mixed-mode laws, i.e. with linear softening, were considered. In this work, the quadratic nominal stress criterion was considered for the initiation of damage. Complete separation is predicted by a linear power law form of the required energies for failure in the pure modes. For full details of the presented model, see reference [10].

3. Results

3.1. Validation with experimental results

In this Section, the results from the experimental tests are presented, followed by the comparison with the CZM strength predictions, for evaluation of this technique.

3.1.1. Experimental results

Figure 3 summarizes the maximum load (P_m) obtained as a function of L_O. The joints have P_m≈27.2 kN for L_O=20 mm. A large P_m increase with L_O was also found because this adhesive has moderate ductility and, therefore, higher loads can be reached by the effect of adhesive plasticization. The percentile increase between the two tested L_O is 43.4%, corresponding to P_m≈39.1 kN for L_O=40 mm. Under these conditions, plasticization of the inner tube was also detected after the tests.

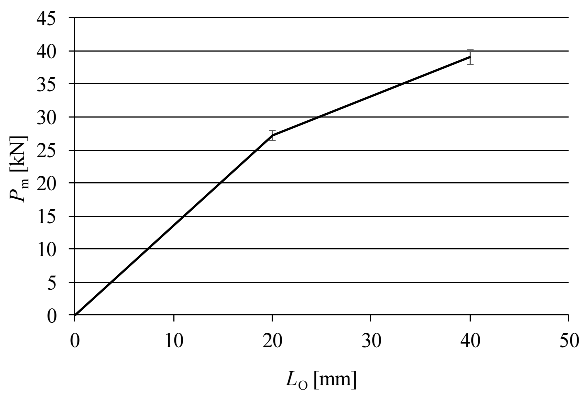

Figure 3. Experimental P_m as a function of L_O for the tubular joints.

3.1.2. Strength prediction by CZM

This study aims to check the validity of CZM in predicting the behaviour of the tubular joints, by the comparison between numerical and average experimental values of P_m. Figure 4 provides this comparison as a function of L_O. The results generally show that the CZM and experimental P_m values are very close for the tubular joints. The percentile difference between the experimental and numerical P_m is 6.1% for L_O=20 mm. This deviation becomes even lower for L_O=40 mm (2.9%). These results clearly show that the triangular CZM model is also accurate. Therefore, the numerical P_m values are accepted, despite the respective dispersion of values.

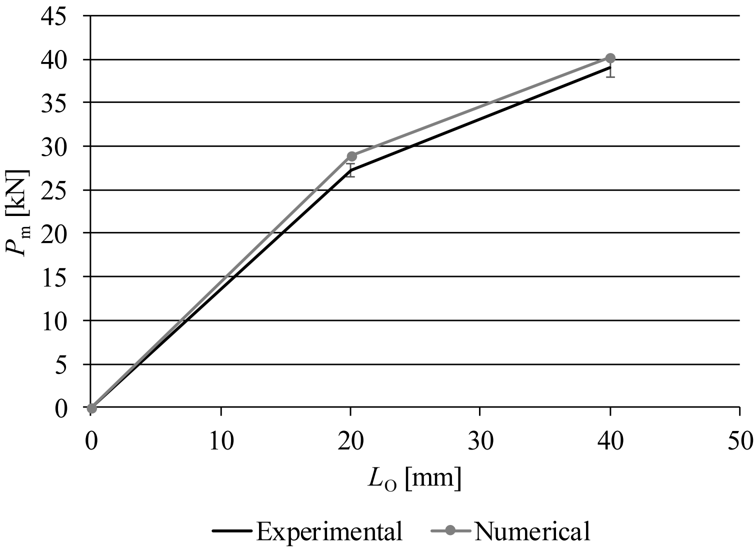

Figure 4. Evaluation of the predicted P_m against the experimental results for the tubular joints.

3.2. Effect of the geometric parameters

L_O and the adherends' thickness were considered. L_O was varied between 10 mm and 50 mm. The parametric analysis considered: (1) change of t_{SI}; (2) variation of t_{SE} and (3) variation of both t_{SI} and t_{SE}. L_O=40 mm was used for all analyses. Moreover, for the studies in which either t_{SI} or t_{SE} is kept constant, its value was fixed at 2 mm.

3.2.1. Overlap length

The variation of L_O is initially addressed numerically. Figure 5 shows the *P*-δ curves obtained by the CZM numerical analysis as a function of L_O. From the evaluation of these curves it is possible to assess P_m and acknowledge its evolution with L_O. The tubular joints showed a linear behavior up to L_O=20 mm.

From L_O=30 mm, the inner aluminum tubes begin to develop massive plastic strains accompanied with their necking (Figure 6), due to the ductility of this adhesive and high loads achieved. This behavior is detected in the *P*-δ curves for L_O=30 mm (reduced necking before failure in the adhesive layer) and L_O=40 and 50 mm (extensive necking).

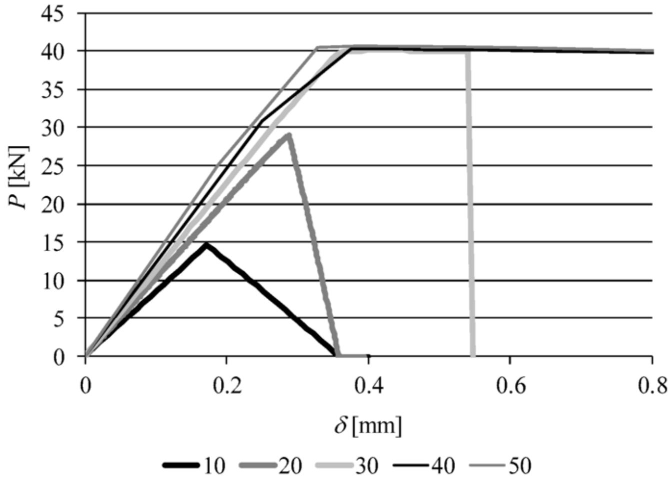

Figure 5. Numerical P-δ curves for the tubular joints as a function of L_O.

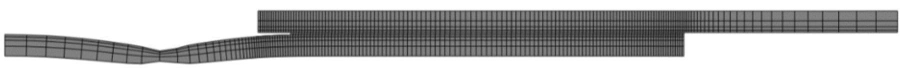

Figure 6. Necking in the inner tube of the tubular joint with L_O=40 mm.

Figure 7 depicts the evolution of P_m with L_O for the tubular joints. The P_m increase between L_O=10 and 20 mm was practically linear (increase of 98.7%), in view of the ductility of the Araldite® 2015, which manages to fail under global yielding conditions for these small L_O. For bigger L_O, failure occurred by necking of the inner tube and, thus, a stabilization of P_m was found. As a result, for the set of geometrical and material conditions tested in this work, there is no advantage in the design with L_O>30 mm.

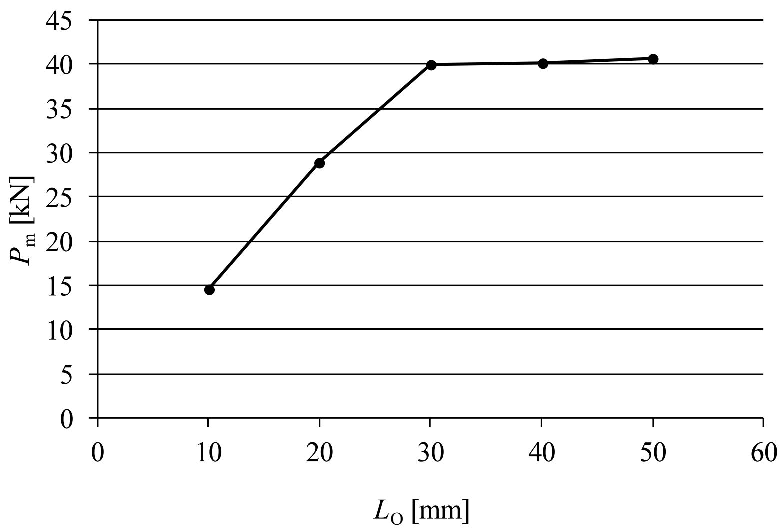

Figure 7. Numerical P_m as a function of L_O for the tubular joints.

3.2.2. Adherends' thickness

As previously described, the adherends' thickness analysis comprises the variation of t_{SI}, t_{SE} and t_{SI} plus t_{SE}. Figure 8 shows the numerical P-δ curves for the tubular joints as a function of t_{SI} (a), t_{SE} (b) and t_{SI} plus t_{SE} (c), obtained by the CZM analysis.

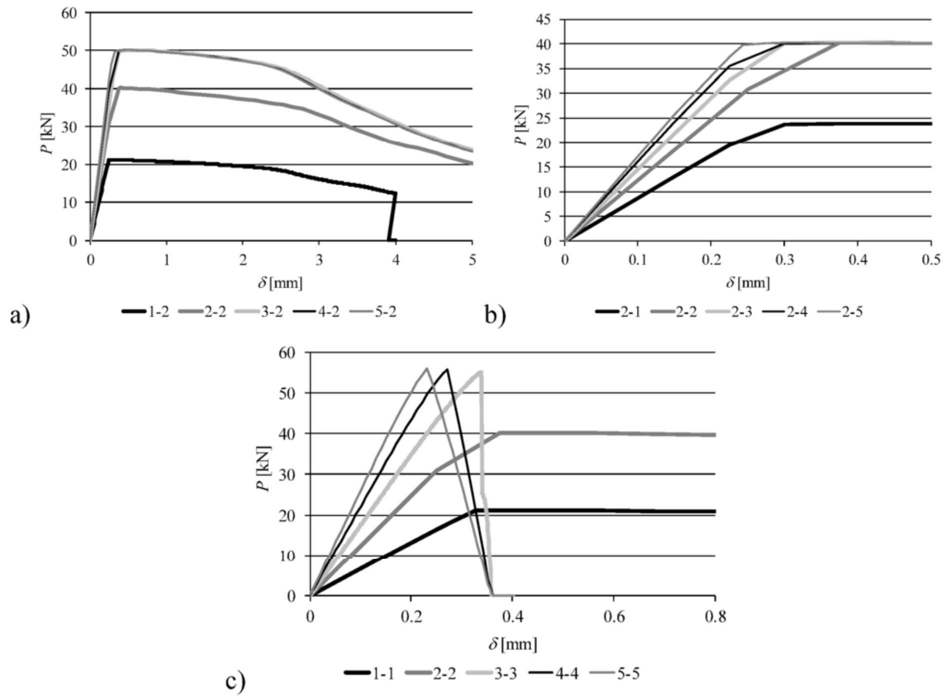

Figure 8. Numerical P-δ curves for the tubular joints as a function of t_{SI} (a), t_{SE} (b) and t_{SI} plus t_{SE} (c).

The P-δ curves relating to the t_{SI} effect show a gradual increase of P_m as t_{SI} increases, but a stabilization of P_m for $L_O \geq 30$ mm. Nonetheless, all P-δ curves point out to necking of the adherends. The tendency was much different for the variation of t_{SE}. Actually, for t_{SE}=1 mm, the tubular joint failed by necking of the outer adherend due to its reduced cross-sectional area, and revealed a major P_m difference to the other t_{SE}. For higher t_{SE}, the behavior was always identical, and failure took place by necking of the inner tube. Finally, for the variation of t_{SI} plus t_{SE}, all failures up to $t_{SI}=t_{SE}$=2 mm occurred by necking of the inner adherend, which has always a smaller cross-sectional area than the outer adherend. The joint with $t_{SI}=t_{SE}$=1 mm showed the worst results, due to the naturally longitudinal tensile strength of the inner tube, which reflected on necking occurrence for smaller applied loads to the joint. P_m increased steadily up to $t_{SI}=t_{SE}$=3 mm but, above this value (inclusively), failure no longer took place in the adherends due to its increased cross-section, but instead by cohesive failure of the adhesive layer. Thus, P_m is identical for $t_{SI}=t_{SE} \geq 3$ mm.

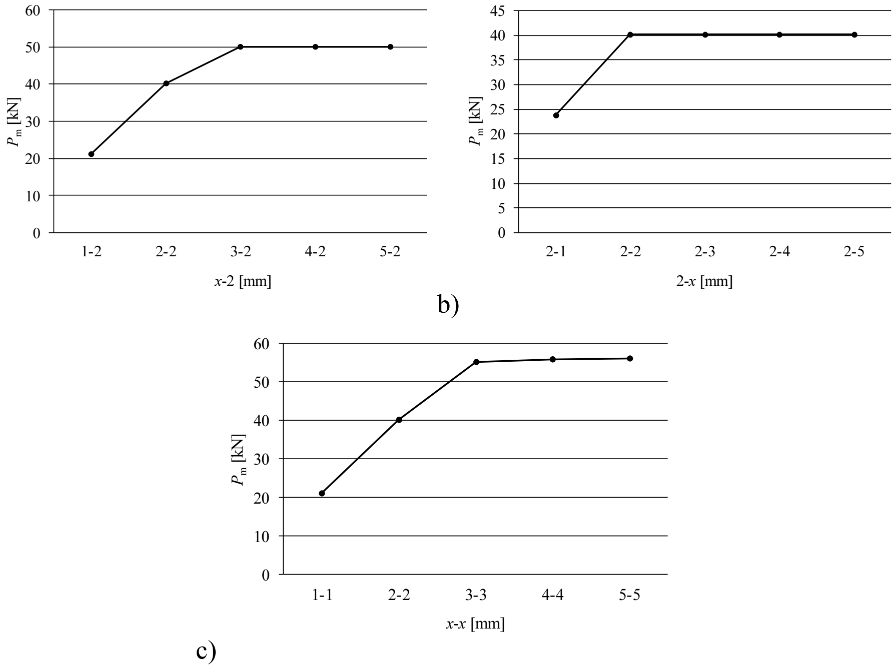

Figure 9. Numerical P_m as a function of t_{SI} (a), t_{SE} (b) and t_{SI} plus t_{SE} (c) for the tubular joints.

Figure 9 depicts the summary of the numerical P_m as a function of t_{SI} (a), t_{SE} (b) and t_{SI} plus t_{SE} (c) for the tubular joints. In accordance with the previous P-δ curves' analysis, for the variation of t_{SI}, no advantage exits in t_{SI}>3 mm, since necking of the outer tube always exists. However, compared to the initial geometry (t_{SI}=t_{SE}=2 mm), a 24.6% strength improvement. The increase of t_{SE} ceased to reflect on P_m for t_{SE}≥2 mm because the traditionally weaker element, the inner tube, is left unchanged. For concurrent variations of t_{SI} and t_{SE}, the inner tube's necking was responsible for joint failure up to t_{SI}=t_{SE}=2 mm. For bigger values of these parameters, cohesive failures of the adhesive were found. Thus, the optimal geometry with identical diameter tubes is t_{SI}=t_{SE}=3 mm.

4. Conclusions

The proposed work addressed the tensile strength of aluminum tubular joints, after validation of the numerical tool with experiments. The experimental tests revealed a large P_m increase with L_O because of the ductility of the Araldite® 2015. The percentile increase between the two tested L_O was 43.4%. For L_O=40 mm, plasticization of the inner tube was detected after the tests. The validation results showed that the CZM and experimental P_m values were very close for the tubular joints. Thus, it was considered that the CZM analysis is suitable to perform the parametric study was undertaken next in the paper. The variation of L_O had a significant influence on P_m. The P_m increase between L_O=10 and 20 mm was practically linear (increase of 98.7%). However, for bigger L_O, failure occurred by necking of the inner tube and, thus, a stabilization of P_m was found. Regarding the tubes' thickness effect, for the variation of t_{SI}, no advantage exits in t_{SI}>3 mm, since necking of the outer tube always exists. The increase of t_{SE} ceased to reflect on P_m for t_{SE}≥2 mm because the traditionally weaker element, the inner tube, is left unchanged. For concurrent variations of t_{SI} and t_{SE}, the inner tube's necking was responsible for joint failure up to t_{SI}=t_{SE}=2 mm. For bigger values of these parameters, cohesive failures of the adhesive were found. Thus, the optimal geometry with identical diameter tubes is t_{SI}=t_{SE}=3 mm.

References

[1] E.M. Petrie, *Handbook of adhesives and sealants*, McGraw-Hill, New York, 2000.
[2] L.F.M.d. Silva, A. Öchsner and R.D. Adams, *Handbook of Adhesion Technology*, Springer-Verlag, Berlin, 2011.
[3] X. He, A review of finite element analysis of adhesively bonded joints, *Int. J. Adhes. Adhes.*, Vol 31, 2011, pp. 248-264.
[4] R.D.S.G. Campilho, M. De Moura, A. Barreto, J. Morais and J. Domingues, Fracture behaviour of damaged wood beams repaired with an adhesively-bonded composite patch, *Composites Part A: Applied Science and Manufacturing*, Vol. 40, 2009, pp. 852-859.
[5] P.B. Woelke, M.D. Shields, N.N. Abboud and J.W. Hutchinson, Simulations of ductile fracture in an idealized ship grounding scenario using phenomenological damage and cohesive zone models, *Computational Materials Science*, Vol. 80, 2013, pp. 79-95.
[6] R. Campilho, M. Banea, J. Neto and L. Da Silva, Modelling of single-lap joints using cohesive zone models: effect of the cohesive parameters on the output of the simulations, *The Journal of Adhesion*, Vol. 88, 2012, pp. 513-533.
[7] E. Dragoni and L. Goglio, Adhesive stresses in axially-loaded tubular bonded joints–Part I: Critical review and finite element assessment of published models, *International Journal of Adhesion and Adhesives*, Vol. 47, 2013, pp. 35-45.
[8] J.L. Lubkin and E. Reissner, Stress Distribution and Design Data for Adhesive Lap Joints Between Circular Tubes, *J. Appl. Mech.*, Vol. 78, 1956, pp. 1213–1221.
[9] R.D.F. Moreira and R.D.S.G. Campilho, Strength improvement of adhesively-bonded scarf repairs in aluminium structures with external reinforcements, *Engineering Structures*, Vol. 101, 2015, pp. 99-110.
[10] R.D.S.G. Campilho, M.D. Banea, A.M.G. Pinto, L.F.M. da Silva and A.M.P. de Jesus, Strength prediction of single- and double-lap joints by standard and extended finite element modelling, *Int. J. Adhes. Adhes.*, Vol. 31, 2011, pp. 363-372.
[11] R.D.S.G. Campilho, M.D. Banea, J.A.B.P. Neto and L.F.M. da Silva, Modelling adhesive joints with cohesive zone models: effect of the cohesive law shape of the adhesive layer, *Int. J. Adhes. Adhes.*, Vol. 44, 2013, pp. 48-56.
[12] T. Faneco, R. Campilho, F. Silva and R. Lopes, Strength and Fracture Characterization of a Novel Polyurethane Adhesive for the Automotive Industry, *J. Test. Eval.*, Vol. 45, 2017, pp. 398-407.
[13] S.L.S. Nunes, R.D.S.G. Campilho, F.J.G. da Silva, C.C.R.G. de Sousa, T.A.B. Fernandes, M.D. Banea and L.F.M. da Silva, Comparative failure assessment of single and double-lap joints with varying adhesive systems, *J. Adhesion*, Vol. 92, 2016, pp. 610-634.
[14] K. Kim, Softening behaviour modelling of aluminium alloy 6082 using a non-linear cohesive zone law, *Proceedings of the Institution of Mechanical Engineers, Part L: Journal of Materials Design and Applications*, Vol. 229, 2015, pp. 431-435.